Atmos. Chem. Phys. Discuss., 10, 4501–4542, 2010
www.atmos-chem-phys-discuss.net/10/4501/2010/


Atmospheric Chemistry and Physics Discussions

This discussion paper is/has been under review for the journal Atmospheric Chemistry and Physics (ACP). Please refer to the corresponding final paper in ACP if available.

# Energetic particle precipitation in ECHAM5/MESSy – Part 2: Solar Proton Events

**A. J. G. Baumgaertner[1], P. Jöckel[1,2], H. Riede[1], G. Stiller[3], and B. Funke[4]**

[1]Max Planck Institute for Chemistry, 55020 Mainz, Germany
[2]now at Deutsches Zentrum für Luft-und Raumfahrt (DLR), Institut für Physik der Atmosphäre, Oberpfaffenhofen, 82234 Weßling, Germany
[3]Institute for Meteorology and Climate Research, Forschungszentrum Karlsruhe, Germany
[4]Instituto de Astrofisica de Andalucia, Granada, Spain

Received: 1 January 2010 – Accepted: 9 February 2010 – Published: 15 February 2010

Correspondence to: A. J. G. Baumgaertner (work@andreas-baumgaertner.net)

Published by Copernicus Publications on behalf of the European Geosciences Union.





## Abstract

The atmospheric chemistry general circulation model ECHAM5/MESSy (EMAC) has been extended by processes that parameterize particle precipitation. Several types of particle precipitation that directly affect $NO_y$ and $HO_x$ concentrations in the middle atmosphere are accounted for and discussed in a series of papers. In part 1, the EMAC parameterization for $NO_x$ produced in the upper atmosphere by low-energy electrons is presented. Here, we discuss production of $NO_y$ and $HO_x$ associated with Solar Proton Events (SPEs). A submodel that parameterizes the effects of precipitating protons, based on flux measurements by instruments on the IMP or GOES satellites, was added to the EMAC model. Production and transport of $NO_y$ and $HO_x$, as well as effects on other chemical species and dynamics during the 2003 Halloween SPEs are presented. Comparisons with MIPAS/ENVISAT measurements of a number of species affected by the SPE are shown and discussed. There is good agreement for $NO_2$, but a severe disagreement is found for $N_2O$ similar to other studies. We discuss the effects of an altitude dependence of the N/NO production rate on the $N_2O$ and $NO_y$ changes during the SPE. This yields a modified parameterization that shows good agreement between MIPAS and model results for $NO_2$, $N_2O$, $O_3$, and HOCl. With the ability of EMAC to relax the model meteorology to observations, accurate assessment of total column ozone loss is also possible, yielding a loss of approximately 10 DU at the end of November. Discrepancies remain for $HNO_3$, $N_2O_5$, and $ClONO_2$, which are likely a consequence from the missing cluster ion chemistry in the EMAC model as well as known issues with the model's $NO_y$ partitioning.

## 1 Introduction

Solar flares and coronal mass ejections are eruptions on the sun's surface that lead to vastly increased fluxes of high-energy particles. Depending on the position of the Earth relative to the ejection, the particles can reach the earth's atmosphere. The



ACPD

10, 4501–4542, 2010



phenomenon is then called a solar proton event (SPE). An SPE causes ionizations, dissociations, dissociative ionizations, and excitations in the atmosphere. This results in the production of $HO_x$ and $NO_y$ in the middle and upper atmosphere (Brasseur and Solomon, 1986; Jackman and McPeters, 2004). The altitude profile of the production is mainly determined by the type and number of precipitating particles and their energy distributions, which then also determines the SPE's significance in terms of associated ozone depletion through catalytic destruction by the $HO_x$ and $NO_x$ products. Such events are interesting natural experiments that allow us to test and improve our understanding of atmospheric chemistry, our observational capabilities, and numerical models.

The effects of SPEs on the middle atmosphere have been measured and modelled extensively for almost four decades, initiated by Weeks et al. (1972). Effects on $NO_x$ chemistry were first presented by Heath et al. (1977). Recently, a review on observational and modeling efforts was presented by Jackman and McPeters (2004). The fourth largest period of SPEs in the past 40 years occurred in October/November 2003 and has been termed Halloween events and received considerable attention. Jackman et al. (2005) investigated both short-term and long-term effects of the Halloween SPEs. 2-D model simulations were compared to NOAA16 SBUV/2 ozone and UARS HALOE $NO_x$ measurements. In the lower and upper mesosphere, short-term ozone depletion up to 50% and greater than 70%, respectively, were found in the model results. Measurements showed a loss of approximately 40% in the lower mesosphere. Northern Hemisphere polar ozone depletion greater than 0.5% was predicted to last for 8 months. SCIAMACHY/ENVISAT measurements of the ozone depletion were shown by Rohen et al. (2005) and Rohen et al. (2006). In addition, Rohen et al. (2005) compared the ozone depletion with results from a 2-D chemistry transport model based on SLIMCAT. In the five weeks following the SPEs the ozone depletion was captured fairly well by the model and agrees approximately with the model results of Jackman et al. (2005).

The MIPAS instrument on board ENVISAT has been used extensively to study ef-



ACPD
10, 4501–4542, 2010



fects of the Halloween SPE on the chemical composition of the middle atmosphere. For example, effects on $NO_x$ and ozone are shown in López-Puertas et al. (2005a), von Clarmann et al. (2005) shows HOCl and ClO perturbations, $HNO_3$, $N_2O_5$, and $ClONO_2$ changes are discussed in López-Puertas et al. (2005b), and $N_2O$ enhancements are discussed by Funke et al. (2008). Jackman et al. (2008) noted that MIPAS measurements of the $HNO_3$ enhancements were unexpectedly large; Verronen et al. (2008) attributed them to ion-ion recombination between $NO_3^-$ and $H^+$.

Jackman et al. (2007) discussed dynamical effects in the mesosphere using results from the TIME-GCM model. SPE-induced temperature anomalies up to 2.6 K were found and background wind velocities changed up to 25%.

The present study discusses the immediate effects of the Halloween SPEs using results from simulations with the ECHAM5/MESSy model system with an additional submodel that parameterizes the effects of SPEs in the middle atmosphere. The model results are evaluated using data from the MIPAS instrument. Disagreements between model and satellite data are attempted to reconcile using several different options.

The model and the satellite instrument are described in Sects. 2 and 3, respectively. The simulated time evolution of several trace gases affected by the SPE as well as comparisons with the satellite observations are described in Sect. 4. Options for improvements to the parameterization are presented, and the remaining discussion is based on the parameterization that yields the best results when compared to the MIPAS measurements. Finally, a summary and conclusions are presented in Sect. 5.

## 2 Model description

### 2.1 ECHAM5/MESSy

The ECHAM/MESSy Atmospheric Chemistry (EMAC) model is a numerical chemistry and climate simulation system that includes sub-models describing tropospheric and middle atmosphere processes and their interaction with oceans, land and human in-





fluences (Jöckel et al., 2006). It uses the Modular Earth Submodel System (MESSy, see Jöckel et al., 2005; Jöckel et al., 2010) to link multi-institutional computer codes. The core atmospheric model is the 5th generation European Centre Hamburg general circulation model (ECHAM5, Roeckner et al., 2006). The model has been shown to consistently simulate key atmospheric tracers such as ozone (Jöckel et al., 2006), water vapour (Lelieveld et al., 2007), and lower and middle stratospheric $NO_y$ (Brühl et al., 2007). For the present study we applied EMAC (ECHAM5 version 5.3.02, MESSy version 1.8$^+$) in the T42L90MA-resolution, i.e. with a spherical truncation of T42 (corresponding to a quadratic Gaussian grid of approximately 2.8 by 2.8 degrees in latitude and longitude) with 90 vertical hybrid pressure levels up to 0.01 hPa. This part of the setup matches the model evaluation study by Jöckel et al. (2006). Enabled submodels are also the same as in Jöckel et al. (2006) apart from the new submodels SPE and SPACENOX, and the sub-submodel FUBRad (Nissen et al., 2007), a high-resolution short-wave heating rate parameterization. The submodel SPACENOX, dealing with $NO_x$ production from low-energy electrons in the upper atmosphere, is described in the companion paper (Baumgaertner et al., 2009), SPE is described here. The chosen chemistry scheme for the configuration of the submodel MECCA (Sander et al., 2005) is simpler compared to the configuration in Jöckel et al. (2006). For example, the NMHC chemistry is not treated at the same level of detail. The complete mechanism is documented in the supplement.

The basic state of the model atmosphere is determined by a set of boundary conditions in order to make comparisons with observations more meaningful. Sea surface temperatures are taken from the Met Office Hadley Centre (HadISST), the equatorial zonal wind is weakly relaxed towards observed winds to yield the correct phase of the QBO. Long lived trace gases are relaxed towards observed concentrations at the surface, short lived species are emitted into the lowermost model layers (Baumgaertner and Brühl, 2008). The model can be nudged towards analyzed meteorology (ECMWF ERA-40), allowing direct comparisons with measurements. Results from setups that were nudged in the troposphere between 200 and 700 hPa as well as from free-running

setups will be shown here.

### 2.2 The submodel SPE

The new submodel with the name SPE parameterizes the effects of energetic protons by calculating ionization rates and, subsequently, production rates of $NO_x$ and $HO_x$. The results are added to the model tendencies of $NO_x$ and $HO_x$.

For the calculation of ionization rates a method based on Vitt and Jackman (1996) was employed. The proton flux measurements by GOES (Geostationary Operational Environmental Satellite) or IMP (Interplanetary Monitoring Platform) are interpolated to a logarithmic energy spectrum. The energy deposited in any model layer is calculated directly using the thicknesses of the considered layer and an energy-range relationship. Here, we used the relationship by Bethe and Ashkin (1953),

$$R = (E/a)^b \quad (1)$$

where $R$ is the range in meters and $E$ is the particle energy measured in MeV. Bethe and Ashkin (1953) determined $a=9.3$ and $b=1.8$. In order to evaluate the ionization rate calculation, the SPE submodel was employed in a column mode and the simulation results were compared to published ionization rates. For this, daily ionization rates provided by Jackman (2006) for the SOLARIS working group of SPARC (Stratospheric Processes and their role in climate, a project of the WCRP – World Climate Research Programme) were used as a reference. Resulting ozone depletion and other SPE effects can then be compared without large uncertainties in the underlying ionization rates. Figure 1 depicts the column model ionization rates (black lines) averaged over 28 October 2003 (dashed line) and 29 October (solid line) using hourly model output, and the data by Jackman (2006) (blue lines) for the same days. Although there is general agreement, the ionization rate altitude dependence is not satisfactory; at 45 km on 29 October for example an overestimation of approximately 50% is found. However, a correct altitude dependence is crucial due to the steep profiles of ozone and other constituents that the SPE affects. Therefore, a series of sensitivity studies was performed





using different sets of $a$ and $b$ in Eq. 1. Values for $a$ between 9 and 14, for $b$ between 1 and 3 were tested. Using $a = 12.3$ and $b = 1.8$ yield the best agreement between the calculated and published ionization rates. The results are shown as the red lines in Fig. 1. Because of the better agreement with the results by Jackman (2006) who used a more complex approach, this set of parameters was employed for the rest of this study. Note that the agreement above 50 km is affected by the different resolution of the data sets: the vertical resolution of EMAC in the L90 setup degrades to 8 km at the highest altitude.

Instead of using internally calculated ionization rates, externally calculated rates, 1-D or 3-D, generally with a lower time resolution compared to the online calculation, can also be applied. This option was however not used in the present study.

Since the magnetic field lines guide the charged particles toward the geomagnetic poles, full ionization was only applied poleward of 60° geomagnetic latitude. The production of N and NO was parameterized using commonly cited values of 0.55 N atoms and 0.7 NO molecules per ion pair (e.g., Jackman et al., 2005) because the model does not incorporate excited state chemistry of atomic nitrogen. However, in an attempt to improve the agreement between satellite and model results, we tested a height dependent N/NO production efficiency which is described in Sect. 4.1. The more complicated production of H and OH by ionization was parameterized using an approximation to data published in Solomon et al. (1981). $HO_x$ production per ion pair depends on altitude and the baseline ionization rate. The altitude dependence was approximated as

$$f(h) = 2 - \exp(h - 83)/6, \quad (2)$$

where $h$ is the altitude in km. Using thresholds $t(q)$ as in Solomon et al. (1981) for the baseline ionization rate dependence, the production rates $H^{prod}$ and $OH^{prod}$ are then

$$(H^{prod}, OH^{prod}) = 0.5 \cdot q \cdot f(h) \cdot t(q) \quad (3)$$

where $q$ is the ionization rate.



ACPD
10, 4501–4542, 2010



### 2.3 The CAABA boxmodel

We also performed simulations with the atmospheric chemistry box model CAABA (Chemistry of the Atmosphere As a Box model Application, version 2.4d), described in Sander et al. (2010). CAABA contains the chemistry module MECCA (Sander et al., 2005) and the photolysis module JVAL (based on Landgraf and Crutzen, 1998), which are also part of EMAC, therefore the chemical and photochemical schemes are almost identical to the 3-D simulations.

## 3 Satellite observations

The Halloween SPE effects on atmospheric chemistry have been observed by instruments on board the Environmental Satellite (ENVISAT). Here, we present measurements from the limb viewing spectrometer MIPAS (Michelson Interferometer for Passive Atmospheric Sounding) to assess if the SPE-induced production of trace gases and subsequent ozone depletion as seen in the model output are realistic. MIPAS observations of the Halloween SPE have previously been presented for example by López-Puertas et al. (2005a), López-Puertas et al. (2005b), von Clarmann et al. (2005) and Funke et al. (2008). Only MIPAS spectra version V3O were employed. The employed baseline versions are listed in Table 1.

When several versions were available for a specific day, the newest version was employed. To facilitate comparison with the model results, the MIPAS data were binned to create a daily time series. The data were also gridded onto the EMAC model grid used here (T42). In the vertical, the original geometric height grid was adopted as is. For comparison with the MIPAS data, the model output was transferred onto the same vertical grid using the simulated geopotential height.

The vertical resolution of the MIPAS data is generally lower than the model vertical resolution. Therefore, the model results were convolved with the corresponding MIPAS averaging kernel (AK) if not noted otherwise.



ACPD
10, 4501–4542, 2010



## 4 Results and discussion

The SPE submodel has been tested with EMAC for the time of the Halloween SPEs between 28 October and 4 November 2003. For the most intense period, 28–31 October 2003, the zonally averaged (70°–90° N) ionization rate profiles are depicted as a function of time in Fig. 2. The major episode of the SPE starts at approximately 12:00 UTC on 28 October 2003. Above 40 km altitude the ionization rate exceeds 10 000 ion pairs $cm^{-3}$ $s^{-1}$ for several hours on 29 October 2003. Less intense periods follow on the 30 October and 2–4 November. There is excellent agreement with the ionization rates calculated by Jackman et al. (2005), see their Fig. 3.

In addition to the simulation with the SPE submodel switched on (denoted S-SPE in this paper), one simulation was performed without the submodel (denoted S-NOSPE). This allows to accurately assess the impact of the SPE by comparing the two simulations with each other. Both simulations were nudged towards the observed meteorology in the troposphere, so differences in the dynamics of the two simulations are small.

Before we present an analysis of trace gases that are affected by the Halloween SPEs, we discuss the simulated and observed temperatures before and during the events. Because many reactions involving $NO_y$ species are temperature dependent, it is important to know how accurately the temperature is simulated by the model. In Fig. 3 the EMAC temperatures between 26 October and 30 November 2003 are directly compared to MIPAS measurements at altitudes between 38 and 66 km at 4 km intervals. All altitude bins can be distinguished by a different colour and symbol and are labelled accordingly. In the upper stratosphere between 46 and 54 km a high bias of approximately 10 K can be noted (the model stratopause is situated at approximately 53 km, not shown). Higher up, the model shows a low bias increasing with altitude to 10 K at 66 km. These biases indicate that the model stratopause is lower than in the observations and are likely to affect the comparisons of simulated and measured trace gas concentrations, therefore sensitivity studies using a boxmodel with fixed tempera-



ACPD
10, 4501–4542, 2010



tures are presented in Sect. 4.1.

Atomic nitrogen (N) and nitric oxide (NO) are among the direct products of the SPE, and the effects on $NO_x$ are discussed and evaluated next. Figure 4 depicts changes in $NO_2$ with respect to 26 October for 70–90° N from MIPAS measurements (Fig. 4a) and the corresponding model results with the MIPAS $NO_2$ averaging kernel applied (Fig. 4b). There is a good agreement between the SPE related production of $NO_2$ in the model and the MIPAS observations. The maximum production lies in the lower mesosphere, and the downward transport of the enhancements can be seen in both the model results and the measurements. Note that the enhancements in MIPAS data in the upper mesosphere during the second half of November are not related to in-situ production of $NO_x$ but originate in the lower thermosphere and are transported downward. This effect is not subject of the work presented here, but is discussed in the companion paper by Baumgaertner et al. (2009).

The produced $NO_x$ can partially react to form $N_2O$ as has been shown e.g. by Funke et al. (2008). Figure 5 depicts changes in MIPAS and model data similar to the $NO_2$ changes shown above. It is evident that the model production of $N_2O$ by far exceeds that of the enhancements observed by MIPAS. This is a major deficiency of the model performance during this event and has been found in other model simulations as well (Funke et al., 2008). Before the effects on other species are discussed, possible options for improvements to the model or the SPE parameterization are explored in the next section.

### 4.1 Model improvements

The large discrepancy between simulated and observed $N_2O$ could be due to various reasons:

1. reactions not accounted for or unknown, or inaccurate reaction rates,
2. incorrect external parameters that influence the reactions, such as temperature, or

3. inaccurate assumptions about SPE production of N/NO.

A similar discrepancy between MIPAS $N_2O$ and the Canadian Middle Atmospheric Model (CMAM) during the Halloween storm period was reported by Funke et al. (2008). They attempted to resolve this problem by adding to the $N_2O$-forming reaction (reaction G3107 in the MECCA mechanism, see supplement at http://www.atmos-chem-phys-discuss.net/10/4501/2010/acpd-10-4501-2010-supplement.zip)

$$N(^4S) + NO_2 \rightarrow N_2O + O \quad \text{(R1)}$$

the branches

$$N(^4S) + NO_2 \rightarrow NO + NO \quad \text{(R2)}$$

$$N(^4S) + NO_2 \rightarrow N_2 + O_2 \quad \text{(R3)}$$

with 50% of the reaction rate going into the primary branch R1, and 25% each for the Reactions (R2) and (R3). The same modification was implemented in EMAC (see supplement http://www.atmos-chem-phys-discuss.net/10/4501/2010/acpd-10-4501-2010-supplement.zip) and the equivalent simulation to S-SPE was performed, termed S-SPE-FUNKE hereafter. The results for $N_2O$ are shown in Fig. 6. There is generally less $N_2O$ compared to the S-SPE simulation discussed above (Fig. 5), however, a large overestimation persists.

The second possibility listed above refers to external parameters that influence the production of $N_2O$. The Reaction (R1) that forms $N_2O$ after the SPE is temperature dependent with a rate coefficient of

$$k = 5.8 \cdot 10^{-12} \cdot e^{220/T} \quad (4)$$

(see supplement at http://www.atmos-chem-phys-discuss.net/10/4501/2010/acpd-10-4501-2010-supplement.zip), therefore the temperature discrepancy found above (see Fig. 3) could explain some of the overestimations of $N_2O$. This hypothesis is tested by performing sensitivity simulations of the chemistry only. For this, the

boxmodel CAABA, described in Sect. 2.3, is used. CAABA was initialized with the temperature and tracer mixing ratios of the corresponding spatial and temporal location in the 3-D simulation. Note that the temperature is kept constant throughout the CAABA simulation. The solar proton event was simulated by applying the ionization rates that were calculated in the 3-D study. Temperature sensitivity of the reactions was explored by offsetting the temperature $T_{caaba}$ with respect to the 3-D simulation $T_{3-D}$. As an example, the resulting $N_2O$ mixing ratios for a CAABA simulation for 60 km altitude, 0° E, and 75° N are shown in Fig. 7 for the temperature $T_{3-D}$ (black), as well as for $T_{3-D} + 10$ K (red) and $T_{3-D} + 20K$ (green). The crosses denote MIPAS measurements in the area 75°N±5° latitude.

As expected from the 3-D simulation with the same chemical mechanism, there is a sharp increase of $N_2O$ during the SPE, but no change in the following weeks since there is no $N_2O$ photolysis and no $O(^1D)$ present to deplete $N_2O$. A significant temperature dependence of the amount of $N_2O$ produced is evident. However, mixing ratios are still strongly overestimated when compared to the MIPAS observations.

Finally, we discuss the third possibility, referring to inaccurate assumptions about the production efficiency of N and NO per ion pair. The chemistry submodel MECCA does not contain excited state chemistry required to form $N(^4S)$ and NO from the initial excited states of $N_2$, N, $O_2$ and O (Rusch et al., 1981). Therefore, the common production efficiency of 0.55 N and 0.7 NO per ion pair was applied as mentioned above, although published estimates of the number of $NO_y$ constituents range from 0.33 (Warneck, 1972) to 2.5 (Fabian et al., 1979). The observed discrepancy of $N_2O$ could possibly be resolved by changing these values since the amount of produced $N_2O$ is mostly dependent on the amount of available N atoms. Reducing the number of N atoms produced by an ion pair would therefore yield better results for $N_2O$. Since the 3-D model is computationally too expensive to perform a large number of tests of other N/NO production efficiencies, the following approach was chosen. The boxmodel CAABA, described in Sect. 2.3, was used to simulate the SPE at MIPAS measurement locations for N and NO production per ion pair ranging from 0 to 1.2 using steps sizes of 0.05. There are



ACPD
10, 4501–4542, 2010



approximately 200 MIPAS profiles of $N_2O$ and $NO_2$ between 31 October and 2 November north of 70°N available, all of which were included in this simulation set. Such a short period was chosen in order to avoid strong contributions by vertical transport, which cannot be captured by CAABA. The simulations were performed at 4 km height intervals starting at 42 km.

For each simulation CAABA was initialized at 27 October, one day before the SPE, with the temperature and tracer mixing ratios of the corresponding spatial and temporal location in the 3-D simulation. As in the CAABA simulations above, the SPE was simulated by applying the ionization rates that were calculated in the 3-D study. The simulation was stopped at the time step closest to the MIPAS measurement. Then the percentage deviations from the MIPAS values of both species were calculated. From all deviations the median was calculated separately for $NO_2$ and $N_2O$. Finally, the two medians were averaged using equal weighting. The entire simulation and processing chain is depicted in Fig. 8. It also shows the average deviations for 58 km altitude. From this, the N and NO productions per ion pair minimizing the total deviation was determined. Figure 9, left, shows the resulting production per ion pair for N (filled circles) and NO (filled squares), also indicating the remaining total deviation in percent. On the right, Fig. 9 shows the ratio of N/NO production.

At 42 km, the remaining total deviation is still large (83%), but is below 10% at 46, 50, and 58 km. At 62 km, where the model vertical resolution and the agreement of the ionization rates (see Fig. 1) degrade, deviations rise again up to 40%. Generally, there appears to be a strong height dependence, with an almost negligible production of N atoms below 45 and above 65 km, which is in disagreement with the generally assumed production parameterization of 0.55 N atoms. Above 55 km the production of NO is also in disagreement with the previously used value of 0.7. This is mainly due to the fact that MIPAS yields only small increases of $NO_2$ and $N_2O$ at these altitudes, despite the large ionization rates present there. This discrepancy can only partially be explained by the MIPAS averaging kernels for $NO_2$ and $N_2O$ and warrants further investigation. Note that the production of N and NO per ion pair, as well as the N/NO



ACPD
10, 4501–4542, 2010



production ratio appear to maximize at approximately the height of the stratopause (see Fig. 3), possibly indicating a temperature dependent production mechanism.

A linear interpolation was performed to obtain N and NO production per ion pair with a resolution of 1 km, also shown in Figure 9 (empty circles and squares). We use these values subsequently in a 3-D EMAC simulation, hereafter called S-SPE-NNOEFF. Except for these height dependent N/NO production coefficients, the simulation was identical to S-SPE.

### 4.2 Evaluation of the improved parameterization

The SPE effects on the polar chemistry in the S-SPE-NNOEFF simulation are now evaluated. Firstly, simulated $NO_2$ (Fig. 10) and $N_2O$ (Fig. 11) are compared to the MIPAS observations similar to the evaluation of the simulation S-SPE above. In the stratosphere and lower mesosphere the location of the peak values of $NO_2$ with respect to time and altitude is similar for EMAC and MIPAS (compare Figs. 10 and 4a). The magnitude of the first maximum at the end of October reaches approximately 50–60 ppbv. The agreement with MIPAS is better compared to the simulation S-SPE, because the maximum between 55 and 60 km is similarly pronounced in the model and the observations, whereas $NO_2$ from simulation S-SPE showed a very broad maximum stretching from 50 to 70 km (Fig. 4b).

The enhancements in $N_2O$ shown in Fig. 11 are drastically reduced compared to the simulation S-SPE (Fig. 4b), and are now in satisfactory agreement with the MIPAS observations (Fig. 5a). The maximum during the SPE is located at around 60 km. In the observations, $N_2O$ enhancements reach 4.5 ppbv, which is only slightly overestimated by the model at approximately 6 ppbv. Therefore, the sensitivity simulations for the N/NO production efficiency appear to have provided a significant improvement for the 3-D EMAC simulation.

### 4.3 Further SPE-induced composition changes

The enhancements of both $NO_x$ and OH results in severe ozone depletion in the polar caps. Fig. 12 shows MIPAS (a) and EMAC S-SPE (b) ozone changes in percent relative to 26 October 2003. Both MIPAS and EMAC S-SPE-NNOEFF results show an ozone depletion of up to 50% in the upper stratosphere. In the mesosphere, short-term ozone depletion exceeds 50%. In the sunlit Southern Hemisphere mesosphere ozone loss is less severe (not shown), which can be explained by differences in the ambient $HO_x$ production (Rohen et al., 2005) and the shorter lifetime of $NO_x$. An additional estimate of ozone depletion is obtained by comparing the EMAC S-SPE-NNOEFF and S-NOSPE simulations, shown in Fig. 12d. It is evident that the SPE related ozone depletion is significant and not an artefact of the illustration technique. However, stratospheric ozone depletion due to the SPE appears to be overestimated by up to 20 percentage points, and contributions to ozone loss from intrinsic processes appear to play a non-negligible role.

Ozone depletion is restricted to altitudes above 35 km, thus the expected impact on total ozone content (TOC) is small. The effect of the SPE on TOC can be estimated by comparing EMAC S-SPE-NNOEFF TOC and S-NOSPE TOC for the area north of 70°N, shown as the solid and dashed line, respectively, in Fig. 13. Before the SPE, both simulations show almost identical behaviour of TOC. From 28 October onwards, a reduction of approximately 5 DU is evident, growing to 10 DU at the end of November. Note that the dominating variations on a timescale of a few days are synchronous because both simulations are nudged to the observed meteorology. The increase in TOC loss during the course of November is likely due to the downward transport of $NO_x$ and associated ozone depletion (see above), becoming more and more important for TOC. This TOC loss is greater than simulated by Vogel et al. (2008), who reported an upper limit of 5.5 DU at the end of November. However, because a different geographical area was used and because of the large influence of natural variations, these results are unlikely to contradict each other.



ACPD
10, 4501–4542, 2010



The OH radical is one of the direct products of SPEs as seen above. The production parameterization leads to short-term enhancements of OH in the upper stratosphere and mesosphere of about 5 ppbv as shown in Fig. 14. MIPAS does not measure OH, but several reactions (e.g. outlined in Jackman et al., 2008) involving $HO_x$ source gases also lead to the buildup of chlorine containing trace gases. For example, von Clarmann et al. (2005) and López-Puertas et al. (2005b) have presented evidence for buildup of HOCl and $ClONO_2$ in the stratosphere using MIPAS observations. Figure 15 depicts measured (left) and simulated (right) HOCl enhancements. As reported by von Clarmann et al. (2005), the enhancement commences at the start of the SPE and decreases exponentially afterwards, such that there is no evidence for HOCl enhancements after 5 November. The maximum of about 0.25 ppbv is located at 40 km. The model reproduces this behaviour well, but overestimates the enhancement by about 0.05 ppbv. For $ClONO_2$, the start of the enhancement is delayed by 1–2 days with respect to the SPE and lasts for several weeks as shown in Fig. 16a. López-Puertas et al. (2005b) attributed this behaviour to the relatively slow reaction of the enhanced $NO_2$ to $ClONO_2$, providing a reservoir for the chlorine containing gases. The model (Fig. 16b) qualitatively reproduces the $ClONO_2$ maximum between 32 and 42 km in the weeks after the SPE, but underestimates the buildup by about 50%.

Figure 17 depicts changes of $N_2O_5$ mixing ratios in the same manner. Qualitatively the model reproduces the slow buildup of $N_2O_5$ centred around an altitude of 40 km. Clearly, the measured enhancements of up to 2 ppbv are overestimated by up to a factor of 5. This discrepancy was present in all simulations (S-SPE, S-SPE-FUNKE and S-SPE-NNOEFF). While the reactions that convert $NO_x$ to $N_2O_5$ are sensitive to temperature, the agreement between MIPAS and EMAC temperature at 40 km (see Fig. 3) implies that the disagreement is not related to temperature effects. The lack of cluster ion chemistry in EMAC could however be a possible reason for the disagreement, although the reaction of $N_2O_5$ with cluster ions forming $HNO_3$ cannot be responsible for the reported overestimation because it occurs below 35 km only (Verronen et al., 2008).



ACPD
10, 4501–4542, 2010



Indeed $HNO_3$ mixing ratios are underestimated, similar to other models (see e.g. Jackman et al., 2008) the EMAC simulations predict only an increase of 0.6 ppbv (see supplement at http://www.atmos-chem-phys-discuss.net/10/4501/2010/acpd-10-4501-2010-supplement.zip), compared to enhancements of 1–2 ppbv reported by López-Puertas et al. (2005b) using MIPAS observations. As discussed by Verronen et al. (2008), the observed increase is probably related to the ion-ion recombination reactions missing in EMAC.

If MIPAS and model $NO_y$ (here: $NO_2 + 2xN_2O_5 + HNO_3 + ClONO_2$) are compared (see supplement Fig. 11, http://www.atmos-chem-phys-discuss.net/10/4501/2010/acpd-10-4501-2010-supplement.zip), a good agreement is found. The model overestimations of $N_2O_5$ and $ClONO_2$ especially toward the end of November compensate the more rapid loss of $NO_2$ in the model. This indicates problems concerning the partitioning within the $NO_y$ family and has already been reported by Brühl et al. (2007).

### 4.4 Dynamical effects

In sunlit areas, the SPE induced perturbance of ozone can potentially lead to temperature changes because of its radiative importance. In order to examine SPE effects on temperature and winds, two further simulations were carried out where the nudging of tropospheric meteorology was turned off. The two simulations are otherwise equivalent to the simulations S-NOSPE and S-SPE-NNOEFF, respectively. The simulations were started on 1 October 2003 from the same initial conditions as all other simulations presented here. For the Halloween events, effects on dynamics are only expected to play a role in the sunlit southern polar area. There, the model predicts an ozone loss of 0.5–1 ppmv, equivalent to 30%–70%, in the lower mesosphere (not shown), but prevalent only during the SPE period. The associated temperature changes in the area 70° S–90° S are depicted in Fig. 18a. An average cooling of up to 2.5 K in the lower mesosphere is evident during the first week after the SPE, similar to the results by Jackman et al. (2007). Around the stratopause the cooling lasts longest and is still

discernible at the end of November. The observed cooling is likely due to the changes in UV absorption. As a consequence, the model predicts a change of 3 m/s in the zonal mean wind (Fig. 18b), maximizing at 70 km. Changes in the meridional wind were not significant (not shown). These dynamical effects will be subject to further analyses in the future.

## 5 Summary and conclusions

A new submodel for the parameterization of solar proton events has been implemented in the atmospheric chemistry general circulation model EMAC and tested for the 2003 Halloween storm period. The chemistry submodel of EMAC is also contained in the box model CAABA, allowing to assess the influence of temperature on SPE-induced changes of chemical species through temperature dependent reaction rates. In addition to this feature, EMAC is also well suited for this type of study because of the possibility to relax the model meteorology to reanalysis datasets and because of its interactive chemistry.

The internal calculation of ionization rates, based on particle flux measurements, was evaluated against published ionization rates. One of the parameters of the employed Bethe energy-range relationship was modified by 30% in order to reach better agreement. MIPAS observations were used to evaluate $NO_2$, $N_2O$, $N_2O_5$, HOCl, $ClONO_2$, and $O_3$ which have all been shown to be affected by SPEs. For $N_2O$ the model overestimates SPE related production grossly. Therefore, the production of N and NO per ion pair was modified using results from box model calculations: CAABA simulations were carried out for all individual MIPAS measurements of $NO_2$ and $N_2O$ during and shortly after the SPEs, employing different N/NO production efficiencies. Using the optimized height dependent production efficiencies in the 3-D model yielded good agreement between EMAC and MIPAS for $NO_2$, $N_2O$ and $O_3$. However, due to problems concerning the $NO_y$ partitioning in the model as well as missing cluster ion chemistry, disagreements persist for $HNO_3$, $ClONO_2$ and $N_2O_5$. Despite these discrepancies the SPE

induced ozone depletion in the polar Northern Hemisphere was shown to be in very good agreement with MIPAS throughout the middle atmosphere. Good agreement of HOCl as an indicator for perturbed $HO_x$ was found. Both the modification of the energy-range relationship as well as the modification of the N/NO production efficiency will need to be tested further in EMAC as well as other general circulation models that include chemistry in order to examine their validity. In case further evidence mounts that such modifications are necessary to reconcile models and observations, further laboratory experiments are also conceivable.

Further results of this study include:

1. Significant changes in chemistry and dynamics already arise due to seasonal variation only, as can be shown by comparing SPE-simulations to an additional simulation without SPE. For example, stratospheric ozone loss reaches 50% at the end of November when compared to ozone before the SPEs, but only 35% when compared to a simulation where the SPE submodel was turned off.

2. The loss of total column ozone amounts to approximately 5 DU immediately after the SPEs. At the end of November, when $NO_x$ and associated ozone loss reach lower altitudes, total column loss approaches 10 DU, an amount similar to natural variability and slightly larger than reported by previous studies.

3. In the Southern Hemisphere, EMAC shows an SPE-induced cooling of about 2.5 K in agreement with another study which included more complex feedbacks that can play a role in the mesosphere-lower-thermosphere.

*Acknowledgements.* This research was funded by the ProSECCO, TIES, and MANOXUVA projects within the DFG SPP 1176 CAWSES. We thank all MESSy developers and users for their support. MIPAS level-1b data were provided by ESA. The particle fluxes were provided by the NOAA GOES team (USA) via their website. We have used the Ferret program (http://www.ferret.noaa.gov) from NOAA's Pacific Marine Environmental Laboratory for creating some of the graphics in this paper.

The service charges for this open access publication have been covered by the Max Planck Society.





## References


Baumgaertner, A. J. G. and Brühl, C.: Emission inventory for CCMVal model simulations 1960–2000, tech. rep., http://www2.mpch-mainz.mpg.de/~abaumg/publications/EmissionsCCMVal.pdf, 2008. 4505

Baumgaertner, A. J. G., Jöckel, P., and Brühl, C.: Energetic particle precipitation in ECHAM5/MESSy1 – Part 1: Downward transport of upper atmospheric $NO_x$ produced by low energy electrons, Atmos. Chem. Phys., 9, 2729–2740, 2009, http://www.atmos-chem-phys.net/9/2729/2009/. 4505, 4510

Bethe, H. and Ashkin, J.: Experimental Nuclear Physics, Volume I, chap. II Passage of Radiations through Matter, John Wiley and Sons, New York, USA, 166–357, 1953. 4506

Brasseur, G. P. and Solomon, S.: Aeronomy of the Middle Atmosphere, D. Reidel Publishing Company, 2nd revised edn., 1986. 4503

Brühl, C., Steil, B., Stiller, G., Funke, B., and Jöckel, P.: Nitrogen compounds and ozone in the stratosphere: comparison of MIPAS satellite data with the chemistry climate model ECHAM5/MESSy1, Atmos. Chem. Phys., 7, 5585–5598, 2007, http://www.atmos-chem-phys.net/7/5585/2007/. 4505, 4517

Fabian, P., Pyle, J. A., and Wells, R. J.: The August 1972 solar proton event and the atmospheric ozone layer, Nature, 277, 458–460, doi:10.1038/277458a0, 1979. 4512

Funke, B., García-Comas, M., López-Puertas, M., Glatthor, N., Stiller, G. P., von Clarmann, T., Semeniuk, K., and McConnell, J. C.: Enhancement of $N_2O$ during the October/November 2003 solar proton events, Atmos. Chem. Phys., 8, 3805–3815, 2008, http://www.atmos-chem-phys.net/8/3805/2008/. 4504, 4508, 4510, 4511

Heath, D. F., Krueger, A. J., and Crutzen, P. J.: Solar Proton Event: Influence on Stratospheric Ozone, Science, 197, 886–889, doi:10.1126/science.197.4306.886, 1977. 4503

Jackman, C. H.: Ionization Rates for 1963-2005 from Solar Proton Events, SOLARIS website http://www.geo.fu-berlin.de/en/met/ag/strat/forschung/SOLARIS/Input_data/index.html, 2006. 4506, 4507, 4525

Jackman, C. H. and McPeters, R. D.: Solar Variability and its Effects on Climate, vol. 141 of Geophysical Monograph, chap. The Effect of Solar Proton Events on Ozone and Other Constituents, 305–319, American Geophysical Union, 2004. 4503

Jackman, C. H., DeLand, M. T., Labow, G. J., Fleming, E. L., Weisenstein, D. K., Ko, M. K. W., Sinnhuber, M., and Russell, J. M.: Neutral atmospheric influences of the solar proton events






in October-November 2003, J. Geophys. Res., 110, A09S27, 10.1029/2004JA010888, doi: 10.1029/2004JA010888, 2005. 4503, 4507, 4509
Jackman, C. H., Roble, R. G., and Fleming, E. L.: Mesospheric dynamical changes induced by the solar proton events in October-November 2003, Geophys. Res. Lett., 34, L04812, doi:10.1029/2006GL028 328, 2007. 4504, 4517
Jackman, C. H., Marsh, D. R., Vitt, F. M., Garcia, R. R., Fleming, E. L., Labow, G. J., Randall, C. E., López-Puertas, M., Funke, B., von Clarmann, T., and Stiller, G. P.: Short- and medium-term atmospheric constituent effects of very large solar proton events, Atmos. Chem. Phys., 8, 765–785, 2008, http://www.atmos-chem-phys.net/8/765/2008/. 4504, 4516, 4517
Jöckel, P., Sander, R., Kerkweg, A., Tost, H., and Lelieveld, J.: Technical Note: The Modular Earth Submodel System (MESSy) – a new approach towards Earth System Modeling, Atmos. Chem. Phys., 5, 433–444, 2005, http://www.atmos-chem-phys.net/5/433/2005/. 4505
Jöckel, P., Tost, H., Pozzer, A., Brühl, C., Buchholz, J., Ganzeveld, L., Hoor, P., Kerkweg, A., Lawrence, M. G., Sander, R., Steil, B., Stiller, G., Tanarhte, M., Taraborrelli, D., van Aardenne, J., and Lelieveld, J.: The atmospheric chemistry general circulation model ECHAM5/MESSy1: consistent simulation of ozone from the surface to the mesosphere, Atmos. Chem. Phys., 6, 5067–5104, 2006, http://www.atmos-chem-phys.net/6/5067/2006/. 4505
Jöckel, P., Sander, R., Kerkweg, A., Sander, R., and Tost, H.: Development cycle 2 of the Modular Earth Submodel System, Geosci. Model Dev. Discuss., in preparation, 2010. 4505
Landgraf, J. and Crutzen, P. J.: An Efficient Method for Online Calculations of Photolysis and Heating Rates., J. Atmos. Sci., 55, 863–878, doi:10.1175/1520-0469(1998)055, 1998. 4508
Lelieveld, J., Brühl, C., Jöckel, P., Steil, B., Crutzen, P. J., Fischer, H., Giorgetta, M. A., Hoor, P., Lawrence, M. G., Sausen, R., and Tost, H.: Stratospheric dryness: model simulations and satellite observations, Atmos. Chem. Phys., 7, 1313–1332, 2007, http://www.atmos-chem-phys.net/7/1313/2007/. 4505
López-Puertas, M., Funke, B., Gil-López, S., von Clarmann, T., Stiller, G. P., Höpfner, M., Kellmann, S., Fischer, H., and Jackman, C. H.: Observation of $NO_x$ enhancement and ozone depletion in the Northern and Southern Hemispheres after the October–November 2003 solar proton events, J. Geophys. Res., 110, A09S43, doi:10.1029/2005JA011050, 2005a. 4504, 4508
López-Puertas, M., Funke, B., Gil-López, S., von Clarmann, T., Stiller, G. P., Höpfner, M., Kell-





mann, S., Mengistu Tsidu, G., Fischer, H., and Jackman, C. H.: $HNO_3$, $N_2O_5$, and $ClONO_2$ enhancements after the October-November 2003 solar proton events, J. Geophys. Res., 110, doi:10.1029/2005JA011051, 2005b. 4504, 4508, 4516, 4517

Nissen, K. M., Matthes, K., Langematz, U., and Mayer, B.: Towards a better representation of the solar cycle in general circulation models, Atmos. Chem. Phys., 7, 5391–5400, 2007, http://www.atmos-chem-phys.net/7/5391/2007/. 4505

Roeckner, E., Brokopf, R., Esch, M., Giorgetta, M., Hagemann, S., Kornblueh, L., Manzini, E., Schlese, U., and Schulzweida, U.: Sensitivity of Simulated Climate to Horizontal and Vertical Resolution in the ECHAM5 Atmosphere Model, J. Climate, 19, 3771, doi:10.1175/JCLI3824.1, 2006. 4505

Rohen, G., von Savigny, C., Sinnhuber, M., Llewellyn, E. J., Kaiser, J. W., Jackman, C. H., Kallenrode, M.-B., Schröter, J., Eichmann, K.-U., Bovensmann, H., and Burrows, J. P.: Ozone depletion during the solar proton events of October/November 2003 as seen by SCIAMACHY, J. Geophys. Res., 110, A09S39, doi:10.1029/2004JA010984, 2005. 4503, 4515

Rohen, G. J., von Savigny, C., Llewellyn, E. J., Kaiser, J. W., Eichmann, K.-U., Bracher, A., Bovensmann, H., and Burrows, J. P.: First results of ozone profiles between 35 and 65 km retrieved from SCIAMACHY limb spectra and observations of ozone depletion during the solar proton events in October/November 2003, Adv. Space Res., 37, 2263–2268, doi:10.1016/j.asr.2005.03.160, 2006. 4503

Rusch, D. W., Gérard, J.-C., Solomon, S., Crutzen, P. J., and Reid, G. C.: The effect of particle precipitation events on the neutral and ion chemistry of the middle atmosphere-I. Odd nitrogen, Planet. Space Sci., 29, 767–774, doi:10.1016/0032-0633(81)90048-9, 1981. 4512

Sander, R., Kerkweg, A., Jöckel, P., and Lelieveld, J.: Technical note: The new comprehensive atmospheric chemistry module MECCA, Atmos. Chem. Phys., 5, 445–450, 2005, http://www.atmos-chem-phys.net/5/445/2005/. 4505, 4508

Sander, R., Baumgaertner, A. J. G., Gromov, S., Harder, H., Jöckel, P., Kerkweg, A., Kubistin, D., Riede, H., Taraborrelli, D., and Tost, H.: The atmospheric chemistry box model CAABA/MECCA-3.0, Geosci. Model Dev., in preparation, 2010. 4508

Solomon, S., Rusch, D. W., Gerard, J. C., Reid, G. C., and Crutzen, P. J.: The effect of particle-precipitation events on the neutral and ion chemistry of the middle atmosphere, 2, Odd hydrogen, Planet. Space Sci., 29, 885–892, 1981. 4507

Verronen, P. T., Funke, B., López-Puertas, M., Stiller, G. P., von Clarmann, T., Glatthor, N., Enell, C.-F., Turunen, E., and Tamminen, J.: About the increase of $HNO_3$ in the stratopause





region during the Halloween 2003 solar proton event, Geophys. Res. Lett., 35, L20809, doi: 10.1029/2008GL035312, 2008. 4504, 4516, 4517
Vitt, F. M. and Jackman, C. H.: A comparison of sources of odd nitrogen production from 1974 through 1993 in the Earth's middle atmosphere as calculated using a two-dimensional model, J. Geophys. Res., 101, 6729–6740, doi:10.1029/95JD03386, 1996. 4506
Vogel, B., Konopka, P., Grooß, J.-U., Müller, R., Funke, B., López-Puertas, M., Reddmann, T., Stiller, G., von Clarmann, T., and Riese, M.: Model simulations of stratospheric ozone loss caused by enhanced mesospheric $NO_x$ during Arctic Winter 2003/2004, Atmos. Chem. Phys., 8, 5279–5293, 2008, http://www.atmos-chem-phys.net/8/5279/2008/. 4515
von Clarmann, T., Glatthor, N., Höpfner, M., Kellmann, S., Ruhnke, R., Stiller, G. P., Fischer, H., Funke, B., Gil-López, S., and López-Puertas, M.: Experimental evidence of perturbed odd hydrogen and chlorine chemistry after the October 2003 solar proton events, J. Geophys. Res., 110, A09S45, doi:10.1029/2005JA011053, 2005. 4504, 4508, 4516
Warneck, P.: Cosmic Radiation as a Source of Odd Nitrogen in the Stratosphere, J. Geophys. Res., 77, 6589–6591, doi:10.1029/JC077i033p06589, 1972. 4512
Weeks, L. H., Cuikay, R. S., and Corbin, J. R.: Ozone Measurements in the Mesosphere During The Solar Proton Event of 2 November 1969., J. Atmos. Sci., 29, 1138–1142, 1972. 4503





**Table 1.** Baseline versions for spectra version V3O of the employed MIPAS data.

| $O_3$ | $HNO_3$ | $N_2O_5$ | $NO_2$ | $N_2O$ | HOCl | $ClONO_2$ |
|---|---|---|---|---|---|---|
| 7, 9 | 8, 9 | 9, 10 | 9, 11 | 12 | 3 | 11, 12 |





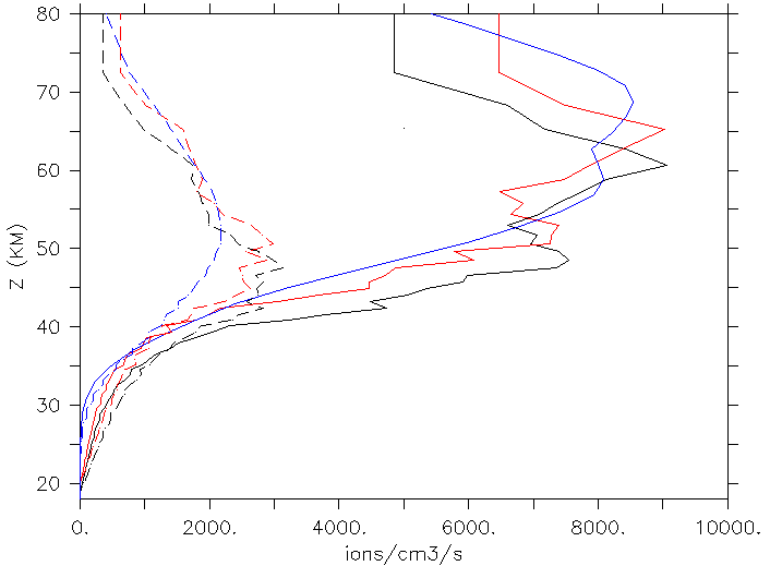


**Fig. 1.** Ionization rates for 28 and 29 October 2003 (dashed and solid lines, respectively) calculated by a column mode version of the SPE submodel using the original (black) and optimized (red) parameters for the energy-range relationship. Results provided by Jackman (2006) are shown in blue.



ACPD
10, 4501–4542, 2010



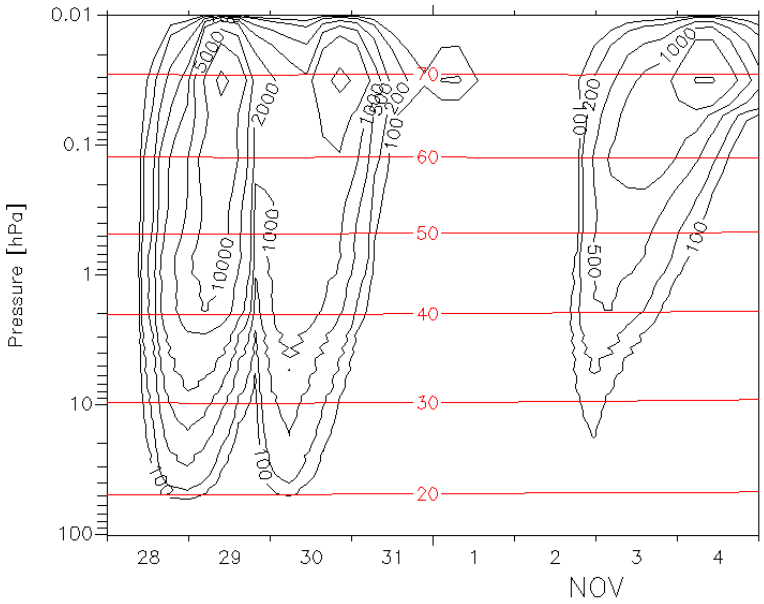


**Fig. 2.** Calculated high-latitude (70°–90° N zonal average) ionization rates (#cm$^{-3}$ s$^{-1}$) during October and November 2003. The red lines denote the altitude in km.



ACPD
10, 4501–4542, 2010



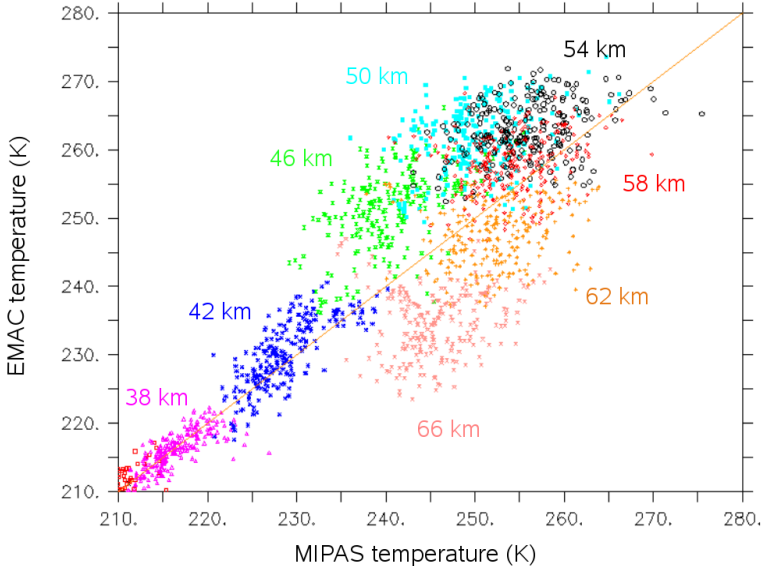


**Fig. 3.** Comparison of zonal average temperatures of MIPAS and EMAC for 70–90° N for 26 October–30 November 2003.



ACPD
10, 4501–4542, 2010



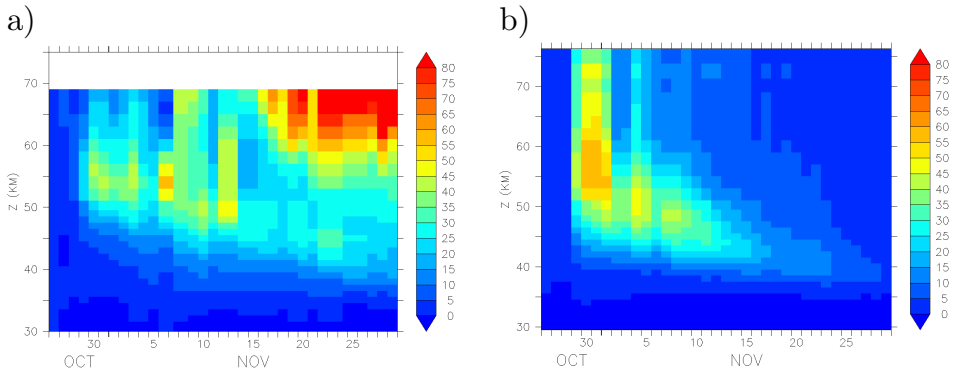


**Fig. 4.** $NO_2$ change (ppbv) with respect to 26 October for 70–90° N for **(a)** MIPAS, **(b)** EMAC simulation S-SPE.



ACPD
10, 4501–4542, 2010



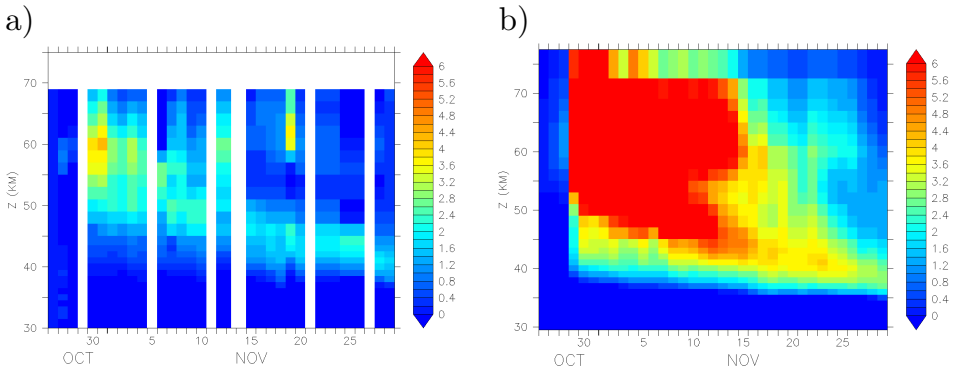


**Fig. 5.** Same as Fig. 4 but for $N_2O$ (ppbv).



ACPD
10, 4501–4542, 2010



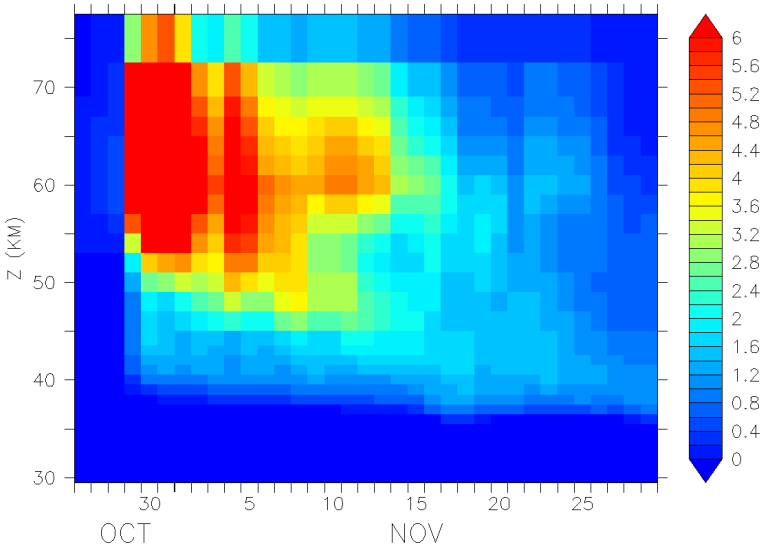


**Fig. 6.** $N_2O$ change (ppbv) in EMAC simulation S-SPE-FUNKE with respect to 26 October for 70–90° N.



ACPD
10, 4501–4542, 2010



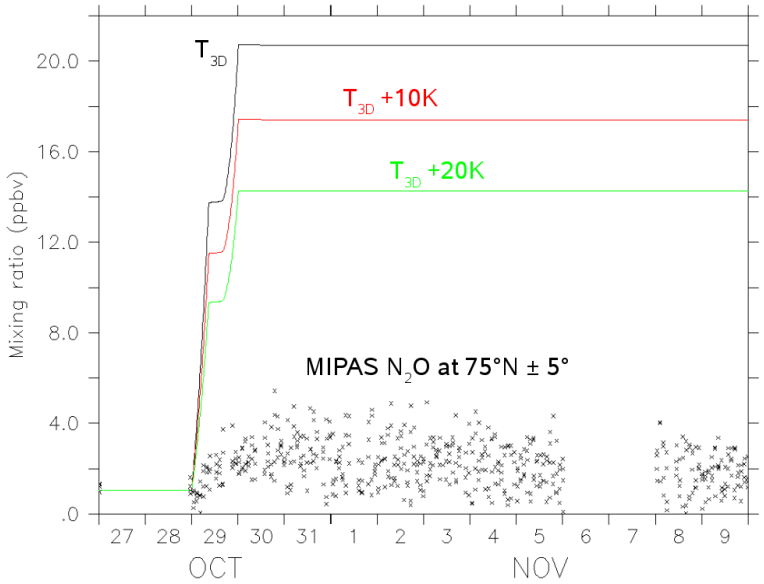


**Fig. 7.** Mixing ratios of $N_2O$ at 60 km, 75° N from the CAABA box model at three different temperatures (lines), and MIPAS $N_2O$ measurements for the same latitude region.



ACPD
10, 4501–4542, 2010



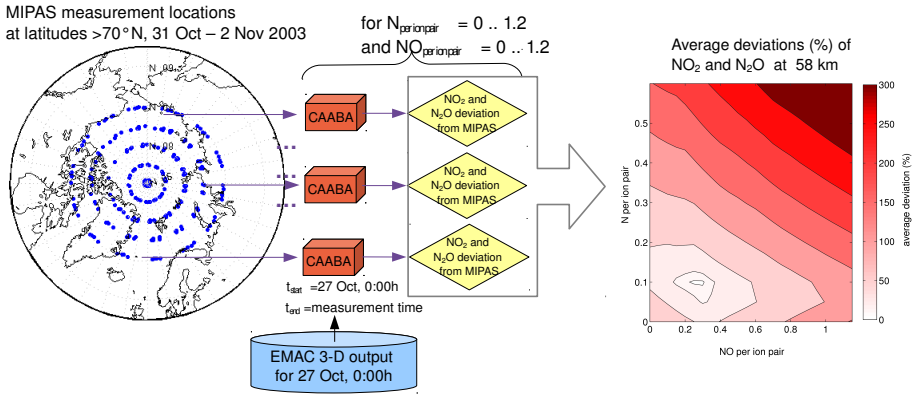


**Fig. 8.** Datasets, simulations, and postprocessing used to determine the N and NO production per ion pair that fits best to MIPAS observations. The depicted processing chain is performed for each altitude separately.



ACPD
10, 4501–4542, 2010

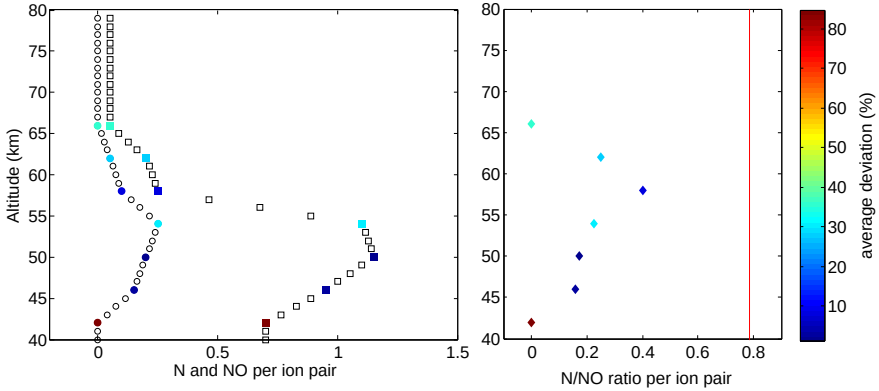


**Fig. 9.** Left: N (filled circles) and NO (filled squares) production efficiencies determined from CAABA simulations. The colour indicates the average deviation from the MIPAS measurements in percent. Empty circles and squares show the linearly interpolated production efficiencies used in the EMAC model simulations S-SPE-NNOEFF. Right: N/NO ratio per ion pair from CAABA simulations (diamonds) and commonly used value (red line).



ACPD
10, 4501–4542, 2010



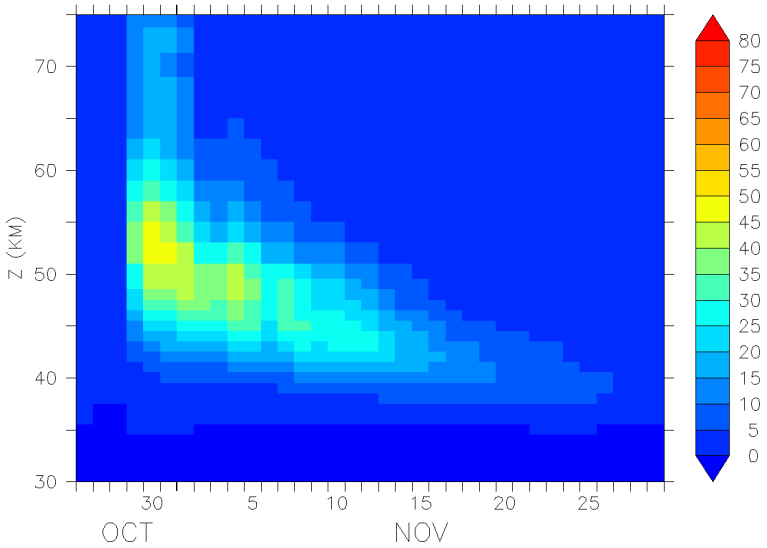


**Fig. 10.** $NO_2$ changes (ppbv) for 70–90° N relative to 26 October 2003 for simulation S-SPE-NNOEFF.



ACPD
10, 4501–4542, 2010



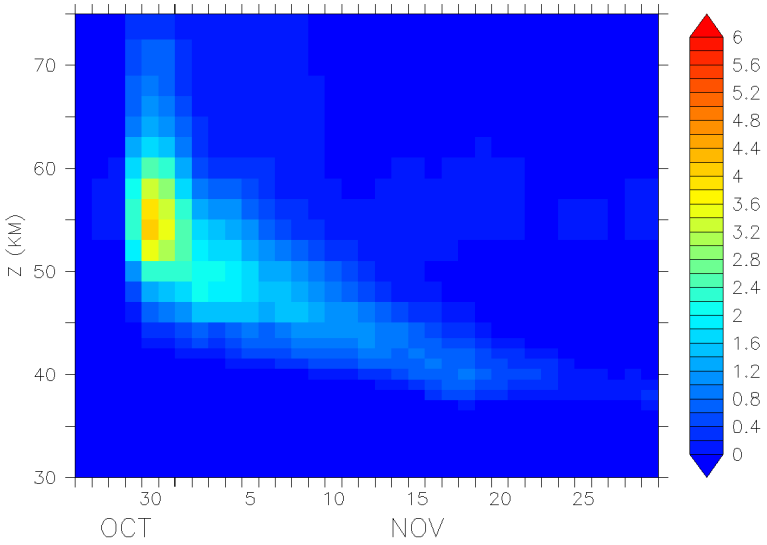


**Fig. 11.** Same as Fig. 10 but for $N_2O$ changes (ppbv).



ACPD
10, 4501–4542, 2010



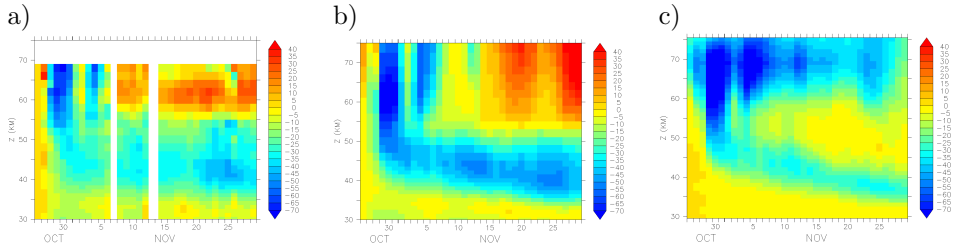


**Fig. 12.** Ozone mixing ratio percentage change; **(a)** MIPAS, relative to 26 October, **(b)** EMAC S-SPE-NNOEFF, relative to 26 October, **(c)** difference between EMAC S-SPE-NNOEFF and S-NOSPE.



ACPD
10, 4501–4542, 2010



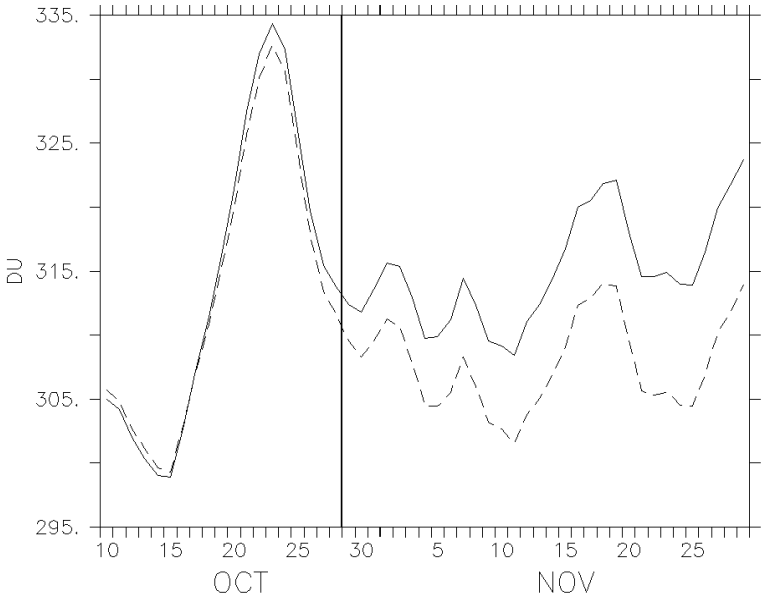


**Fig. 13.** Change of total ozone between the simulations S-SPE and S-NOSPE in the region 70–90° N.



ACPD
10, 4501–4542, 2010



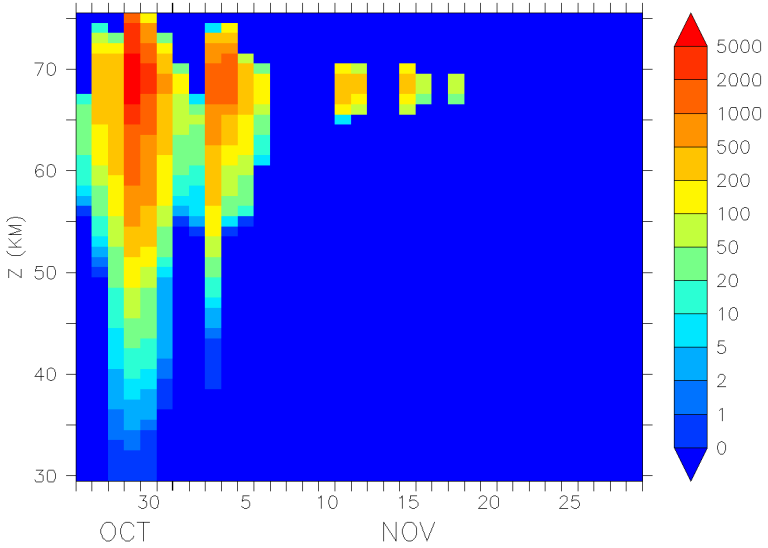


**Fig. 14.** Simulated change (pptv) of OH for 70–90° N with respect to 26 October 2003.



ACPD
10, 4501–4542, 2010



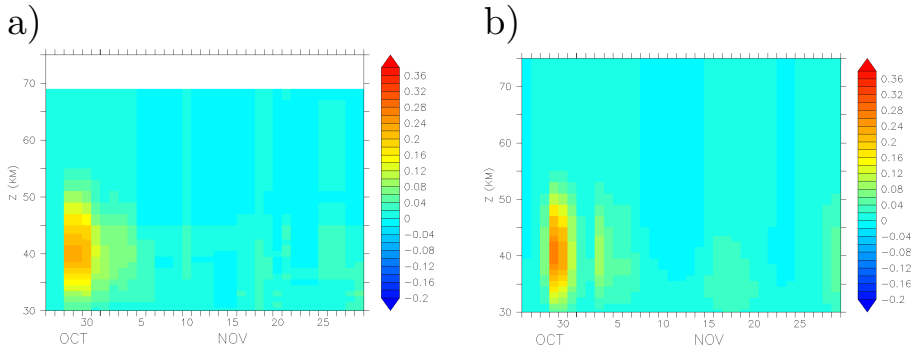


**Fig. 15.** HOCl changes (ppbv) for 70–90° N relative to 26 October 2003; **(a)** MIPAS, **(b)** EMAC simulation S-SPE-NNOEFF.



ACPD
10, 4501–4542, 2010



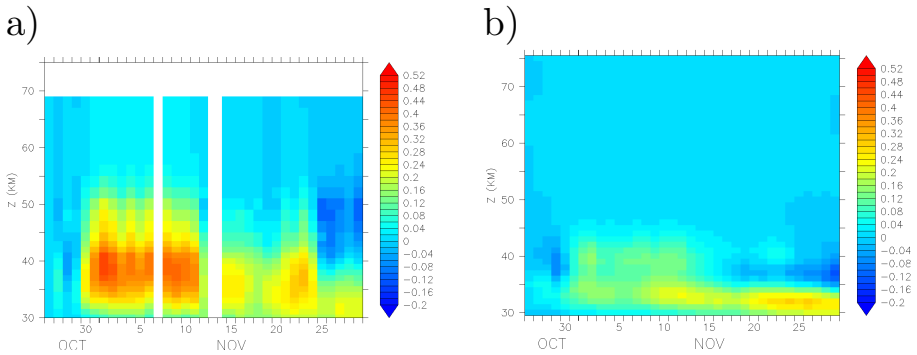


**Fig. 16.** $ClONO_2$ changes (ppbv) for 70–90° N relative to 26 October 2003; **(a)** MIPAS, **(b)** EMAC simulation S-SPE-NNOEFF (here, the MIPAS averaging kernel was not applied).



ACPD
10, 4501–4542, 2010



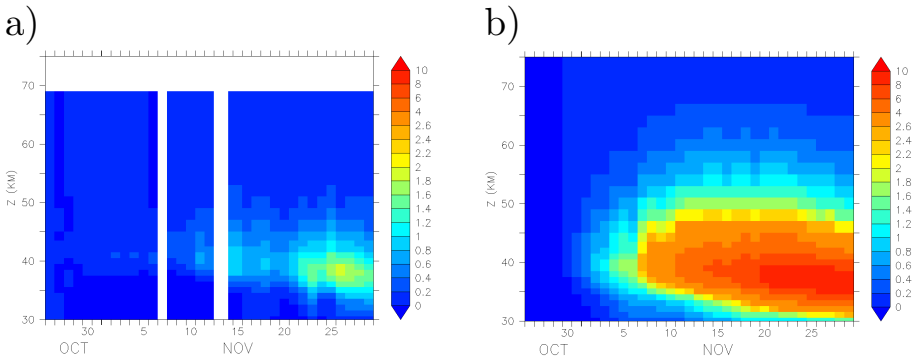


**Fig. 17.** $N_2O_5$ changes (ppbv) for 70–90° N relative to 26 October 2003; **(a)** MIPAS, **(b)** EMAC simulation S-SPE-NNOEFF.



ACPD
10, 4501–4542, 2010



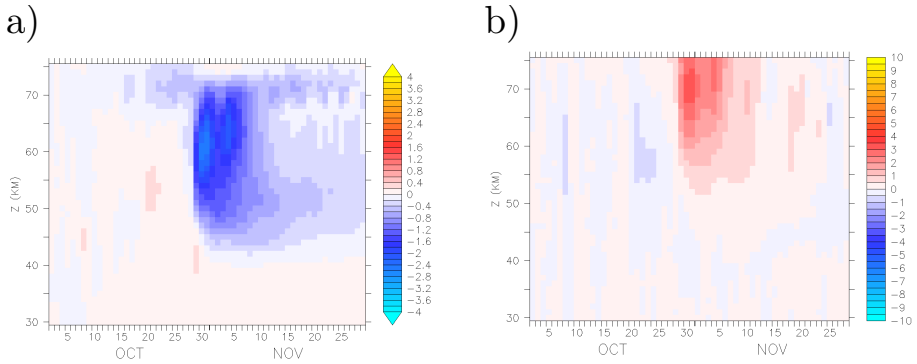


**Fig. 18. (a)** Change of temperature (K) between two free running simulations with and without SPE submodel turned on. **(b)** Change of zonal mean wind (m/s).



ACPD
10, 4501–4542, 2010